國　立　交　通　大　學

電　控　工 程 研 究 所

碩 士 論 文

應用向量次序統計與模糊梯度於彩色影像之自動邊緣偵測

Applying Vector Order Statistics and Fuzzy Gradient to Automatic Edge Detection of Color Images

研　究　生 ： 劉品宏

指 導 教 授： 張 志 永

中 華 民 國 九十九 年 七 月

應用向量次序統計與模糊梯度於彩色影像之自動邊緣偵測

Applying Vector Order Statistics and Fuzzy Gradient to Automatic Edge Detection of Color Images

學　　生：劉品宏　　Student : Pin-Hung Liou

指導教授：張志永　　Advisor : Jyh-Yeong Chang

國立交通大學

電機工程學系

碩士論文

A Thesis

Submitted to Department of Electrical Engineering

College of Electrical and Computer Engineering

National Chiao-Tung University

in Partial Fulfillment of the Requirements

for the Degree of Master in

Electrical and Control Engineering

July 2010

Hsinchu, Taiwan, Republic of China

中 華 民 國 九 十 九 年 七 月

應用向量次序統計與模糊梯度於彩色影像之自動邊緣偵測

學生:劉品宏　　指導教授: 張志永博士

國立交通大學電機與控制工程研究所

摘要

本論文，提出改進基於向量次序統計之彩色邊緣偵測技術的方法，我們的邊緣偵測方法包含兩個部份，首先，第一部份利用模糊梯度的概念來估測每個處理像素的梯度方向，並且根據此方向來調整相對應的視窗方位；第二部部分依向量次序統計計算向量平均距離(VMD)，如此一來，整合了向量次序統計與模糊梯度的偵測方法能夠產生更為穩健的邊緣偵測響應。更進一步，我們將此技術整合到我們所提出的門檻偵測方法，此方法依據影像內容自動作最佳化調整門檻，而不需要手動選取。由測試彩色合成影像與實際影像的數據顯示，我們的自動彩色邊緣偵測是非常方便與可靠的。

Applying Vector Order Statistics and Fuzzy Gradient to Automatic Edge Detection of Color Images

STUDENT: Pin-Hung Liou ADVISOR: Dr. Jyh-Yeong Chang

Institute of Electrical and Control Engineering
National Chiao-Tung University

ABSTRACT

In this thesis, we have proposed an improvement of color edge detector based on vector order statistics. The proposed detector consists of two stages. In the first stage, we use the concept of fuzzy gradient to estimate the direction of the gradient for every processing pixel in the image and adjust the corresponding processing window according to this detected direction for reliable edge detection setup. The second stage computes the vector mean distance (VMD) based on vector order statistics. Hence, the proposed detector, which integrates vector order statistics and fuzzy gradient, can provide more robust response for edge detection. Furthermore, we also combine the edge detector to our proposed thresholding method, which can automatically determine an optimal threshold and be adaptive to different image contents without manual intervention. Thus, the excellent results by our proposed edge detection scheme demonstrate that it is very user friendly and confident.

ACKNOWLEDGEMENTS

I would like to express my sincere gratitude to my advisor, Dr. Jyh-Yeong Chang for valuable suggestions, guidance, support and inspiration he provided. Without his advice, it is impossible to complete this research. Thanks are also given to all of my lab members for their suggestion and discussion.

Finally, I would like to express my deepest gratitude to my family for their concern, supports and encouragements.

Contents

List of Figures

List of Tables

Chapter 1 Introduction

1.1 Motivation

Edge detection plays an important role in image processing and computer vision because of high-level image processing tasks such as image segmentation, object recognition, tracking, stereo analysis, and image coding depend on the quality of the edge detection procedure. The performance of these tasks is therefore tremendously affected by the goodness of edge detection. In grayscale edge detection, the Canny edge detector [1] has become a standard. This is partly because its nonmaximal suppression and thresholding with hysteresis stages produce thin, well-connected edge maps. For an image, edges exist at the boundary of objects cannot be detected in grayscale if there are different hues but no changes in intensities since the color cue is lost during grayscale conversion. Objects will be treated like one big object in the scene when they cannot be distinguished in grayscale. In addition, edge detection is sometimes difficult in low contrast images but rather sufficient results can be obtained in color images.

Consequently, the recent attention has been given to the development of color edge detection operators. Humans can differentiate thousands of colors compared to about two dozen shades of gray; hence, grayscale images do not carry all the edge information that human visual system (HVS) can detect. In [2], Novak and Shafer found that luminance component makes up 90% of all edge points in a color image but the remaining 10% can be crucial for subsequent techniques that rely on edges in an image; in some cases the additional information provided by color is of utmost importance. This approach is compatible with that of the HVS where color plays a

significant role in the perception of boundaries. Multi-dimensional nature of color makes it more challenging to detect edges in color images, and often increases the computational complexity threefold compared to gray scale edge detection. Hence, color edge detection algorithms accept from the beginning that all of the efforts are to find the remaining 10% of the edges.

In this thesis, we propose an improvement of color edge detector based on vector order statistics (VOS) [3], [4]. In this approach, we use the concept of fuzzy gradient [5], [6] to estimate the direction of the gradient for every pixel in the image. For using an adjustable window according to the direction of the gradient, it is more exact to calculate the local maximum edge response for every pixel, and an automatic threshold technique is adaptive to threshold the local maximum edge response for the image content.

1.2 Color Edge Detection

In the review paper on color image segmentation, Ruzon and Tomasi [7] go further and group color edge detection methods into three categories: output fusion methods, multidimensional gradient methods and vector methods. Output fusion methods apply single-channel edge detection techniques to each color plane and then combine the results.

In multidimensional gradient methods, the gradients from the individual channels are recombined before the edge decision, giving rise to a single edge estimate. Early work by Scharcanski and Venetsanopoulos [8] is an approach based on the VOS. Trahanias and Venetsanopoulos employed the reduced ordering (R-Ordering) by the VOS edge detectors of [3], [4]. The robust color morphological gradient (RCMG) edge detector [9] identifies the maximum and minimum pixels in one operation,

although it does not distinguish between them. This is in contrast to the VOS edge detectors that sort the pixels in ascending order from the vector median to the vector extremum. The matrices are then summed over all channels and the edge magnitude and direction given by the principal eigenvalue and the related eigenvector, respectively. Variations of this approach have been used by Cumani [10].

The main problem with both output fusion and multidimensional gradient methods is how to combine the channels to give a final result. For example, The simplest VOS operator is the vector range edge detector that measures the distance between the lowest and highest ranked vectors, i.e., the vector median and the vector extremum, respectively. The minimum vector dispersion (MVD) was shown to be the most effective that proposed to increase the robustness to noise . However, the MVD is unable to provide an estimate of edge direction.

1.4 Automatic Thresholding Technique

Thresholding is a fundamental technique applied in many image processing applications. To enable the building of robust machine vision systems, it would be preferable to automate the edge thresholding process which is adaptive to different image contents without manual intervention.

There are many thresholding algorithms published in the literature. The Otsu [11] algorithm is based on discriminant analysis and uses the zeroth-order and the first-order cumulative moments of the histogram for calculating the value of the thresholding level. The Rosin algorithm [12] fits a straight line from the peak of the intensity histogram to the last non-empty bin. The point of maximum deviation between the line and the histogram curve will usually be located at a corner which is selected as the threshold value. The new feature image proposed by Rakesh [13]

makes it easier to determine hysteresis thresholds.

Selecting an appropriate thresholding algorithm can be a difficult task. The problem is that different algorithms typically produce different results since they make different assumptions about the image content. Therefore, we will introduce an automatic thresholding method that can find the best hysteresis thresholds from all possible parameters.

1.5 Thesis Outline

The thesis is organized as follows. Before introducing the technique of our edge detection and automatic thresholding method, the basic concepts concerning the VOS and color edge detector base on VOS are introduced in Chapter 2. In Chapter 3, we describe our method that improve the disadvantage of the color edge detector which is introduced in Chapter 2, and we also in details describe our automatic thresholding method. In Chapter 4, the experiment results of our automatic color edge detection techniques are shown and compared. At last, we conclude this thesis with a discussion in Chapter 5.

Chapter 2 Introduction to Vector Order Statistics and VMD Color Edge Detector

In this chapter, we briefly explain the basic concepts of vector order statistics and VMD (vector mean distance) color edge detector.

2.1 Vector Order Statistics

2.1.1 Vector Order Statistics Review

Scalar order statistics have played an important role in the design of robust signal analysis techniques. This is due to the fact that any outliers will be located in the extreme ranks in the sorted data. Consequently, these outliers can be isolated and filtered out before the signal is further processed. Ordering of univariate data is well defined and has been extensively studied in order statistics [14]. Let the n random variables X_i, $i = 1, 2, \ldots, n$, be arranged in ascending order of magnitude as

$$X_{(1)} \le X_{(2)} \le \ldots \le X_{(n)} \tag{1}$$

Then the i-th random variable $X_{(i)}$ is the so-called ith order statistic. The minimum $X_{(1)}$, the maximum $X_{(n)}$, and the median $X_{(n/2)}$ are among the most important order statistics, resulting the min, the max, and the median filters, respectively.

The concepts are, however, not straightforwardly expanded to multivariate data since there is not any universal way of defining an ordering in multivariate data. There has been a number of ways proposed to perform multivariate data ordering that

are generally classified into the ordering of multivariate data [15]: marginal ordering (M-ordering), reduced or aggregate ordering (R-ordering), partial ordering (P-ordering), and conditional ordering (C-ordering).

2.1.2 Characteristics of Vector Order Statistics

Let X represent a p-dimensional multivariate $X = [X_1, X_2, ..., X_p]^T$ where X_l, $l = 1, 2, \ldots, p$ are random variables and let X^i, $i = 1, 2, \ldots, n$ be an observation of X. Each X^i is a p-dimensional vector $X^i = [X_1^i, X_2^i, ..., X_p^i]^T$.

In M-ordering, the multivariate samples are ordered along each one of the p-dimensions independently. For color signals, this is equivalent to the separable method where each one of the colors is processed independently. The i-th marginal order statistic is the vector $X^{(i)} = [X_1^{(i)}, X_2^{(i)}, ..., X_p^{(i)}]^T$, where $X_r^{(i)}$ is the ith largest element in the r-th channel. The marginal order statistic $X^{(i)}$ may not correspond to any of the original samples $X^1, X^2, ..., X^n$ as it does in one dimension.

In R-ordering, each multivariate observation X^i is reduced to a scalar value d_i according to a distance criterion. A metric that is often used is the generalized distance to some point. The samples are often arranged in ascending order of magnitude of the associated metric value d_i.

In P-ordering, the objective is to partition the data into groups or sets of samples, such that the groups can be distinguished with respect to order, rank, or extremeness. This type of ordering can be accomplished by using the notion of convex hulls. However, the determination of the convex hull is difficult to do in more than two dimensions. Other ways to achieve P-ordering are special partitioning procedures and

thus are not preferred. Another drawback associated with P-ordering is that there is no ordering within the groups and thus it is not easily expressed in analytical terms. These properties make P-ordering infeasible for implementation in digital image processing.

In C-ordering, the multivariate samples are ordered conditionally on one of the marginal sets of observations. This has the disadvantage in digital image processing that only the information in one component (channel) is used.

From the above, it is evident that R-ordering is more appropriate for color image processing than the other vector ordering methods. If we employ as a distance metric the aggregate distance of X^i to the set of vectors $X^1, X^2, ..., X^n$, then

$$d_i = \sum_{k=1}^{n} \left\| X^i - X^k \right\|, \quad i = 1, 2, ..., n \tag{2}$$

where $\| \cdot \|$ represents an appropriate vector norm. The arrangement of the d_is in ascending order $\left(d_{(1)} \le d_{(2)} \le ... \le d_{(n)}\right)$, associates the same ordering to the multivariate X^is.

$$X^{(1)} \le X^{(2)} \le ... \le X^{(n)} \tag{3}$$

In the ordered sequence, $X^{(1)}$ is the vector median of the data samples which is introduced by vector median filters [16]. It is defined as the vector contained in the given set whose distance to all other vectors is a minimum. Moreover, vectors appearing in low ranks in the ordered sequence are vectors centrally located in the population, whereas vectors appearing in high ranks are vectors that diverge mostly from the data population. These samples are generally called “outliers.” It follows that this ordering scheme gives a natural definition of the median of a population and of the outliers of a population.

2.2 VMD Detector

For a color image I of size $m \times n$, each pixel location (i, j) is represented by a three-tuple color vector $I(i, j) = (I_1(i, j), I_2(i, j), I_3(i, j))$, in which $I_p(i, j)$ denoting the p-th component of a color space for $i = 1, 2, ..., m$ and $j = 1, 2, ..., n$. For each pixel location (i, j), by using a 3×3 window, we compute the local sum of distances to describe the relationship between the current pixel vector $I(i, j)$ and its neighboring pixel vectors. Let $d_l(i, j)$ be the local sum of distances for the current pixel vector $I(i, j)$, then

$$d_l(i, j) = \sum_{k=i-1}^{i+1} \sum_{h=j-1}^{j+1} \| I(i, j) - I(k, h) \| \qquad (4)$$

where $\| \cdot \|$ represents a 2-norm. After we have computed the local sum of distances $d_l(i, j)$ of the current pixel location (i, j), we sort the distance values in the neighboring area in ascending order $d_{l(1)} \le d_{l(2)} \le ... \le d_{l(9)}$. The distance values $d_{l(1)}$ and $d_{l(9)}$ correspond to the minimum and the maximum of the nine distance values, respectively.

By the concept of R-ordering, the ordering of $d_{l(1)} \le d_{l(2)} \le ... \le d_{l(9)}$ associates the same ordering to the pixel vectors, $X^{(1)} \le X^{(2)} \le ... \le X^{(9)}$, which means that $X^{(1)}$ is the pixel vector having the smallest local sum of distances and $X^{(9)}$ is the pixel vector having the largest local sum of distances. Therefore, if the current pixel location (i, j) has an edge, the vector $I(i, j)$ must have a larger response of $d_l(i, j)$.

Although we now obtain the information on the smallest and the largest local sum of distances, the information contained among vectors $X^{(1)}, X^{(2)}, ..., X^{(9)}$

should also be captured and be useful for edge detection. The maximal variation among vectors is an indication of the distribution of the nine vectors. Since that vectors $X^{(1)}$, $X^{(2)}$, ..., $X^{(9)}$ correspond to the ordering of the aggregate distances, the confined maximal variation $\mathrm{MV_c}$ among these vectors can be simply defined as

$$MV_c = \max\left(\left\| X^{(i)} - X^{(i+1)} \right\| \right), \quad i = 1, 2, ..., 8 \tag{5}$$

When the value $\mathrm{MV_c}$ is determined, we can also determine the exact two vectors $X^{(i)}$ and $X^{(i+1)}$ which correspond to $\mathrm{MV_c}$. $X^{(i)}$ and $X^{(i+1)}$ further suggest that $X^{(1)}$, $X^{(2)}$, ..., $X^{(9)}$ can be classified into two clusters: (1) vectors, $X^{(1)}$, $X^{(2)}$, ..., $X^{(i)}$, from smaller side of the edge, and (2) vectors, $X^{(i+1)}$, $X^{(i+2)}$, ..., $X^{(9)}$, from larger side of the edge. Let M_s and M_l be the mean vector of the vectors $X^{(1)}$, $X^{(2)}$, ..., $X^{(i)}$, and the vectors $X^{(i+1)}$, $X^{(i+2)}$, ..., $X^{(9)}$ respectively. Thus, VMD can be defined as

$$VMD = \left\| M_l - M_s \right\| \tag{6}$$

VMD detect the variation between two sides of edge (larger and smaller side) by a distance measure. Consequently, in a uniform area, where all vector values are close to each other, the output of VMD will be small. On the other hand, the output of VMD will be large since M_s and M_l are the mean vectors of two sides of the edge.

Chapter 3 The Improvement of VMD Detector and Automatic Threshold Selection

3.1 The Proposed Method

The VMD method suffers from the disadvantage of the weak ability for detecting oblique edges due to the fact that its gradient magnitude is derived from the fixed window with the distance between the mean vector of the large side and the mean vector of the small side. In addition, in the presense of noise and for non-ideal edges, the maximal variation that splits the window into the large side and small side may not represent the distribution among the vectors in the fixed window, and then the VMD may produce an edge response that is not necessarily representative of the real gradient.

To avoid these problems, we use an adjustable window that can rotate its orientation according to the direction of the gradient. In the 3×3 window, we classify the direction of the gradient to four orientations, i.e., $W-E$ direction (0°), $SW-NE$ direction (45°), $S-N$ direction (90°), and $SE-NW$ direction (135°) that can be determined by the fuzzy gradient value which is introduced by the fuzzy image filter [5] and the fuzzy random impulse noise reduction method (FRINR) [6]. Thus, the new proposed method will combine VMD with the fuzzy image filter and FRINR that have the ability to estimate the direction of the gradient for each pixel and adjust the window for more exactly detecting edge response.

In our approach, there are two steps that are used to define the direction of the gradient for each pixel in the color image. First, consider a color image I with size $m\times n$ be represented by color vector $I(i,j)=\left(I_1(i,j),\ I_2(i,j),\ I_3(i,j)\right)$, in which

$I_p(i, j)$ denoting the *p*-th component of a color space, we calculate $g(i, j)$ and $mg(i, j)$ in the 3×3 window as

$$g(i, j)=\frac{\sum_{k=-1}^{1}\sum_{h=-1}^{1}\left\| I(i+k, j+h)-I(i, j) \right\|}{8} \tag{7}$$

$$mg(i, j)=\frac{\sum_{k=-1}^{1}\sum_{h=-1}^{1}\left\| g(i+k, j+h)-g(i, j) \right\|}{8} \tag{8}$$

where $\|\cdot\|$ represents a 2-norm and (i, j) represents the *i*-th row and *j*-th column in the color image *I*. Because edge pixels and corrupted impulse noise pixels generally cause large $g(i, j)$ value, we also calculate $mg(i, j)$ that can help us to distinguish edge pixels and noise pixels. To discriminate edge pixels and noise pixels, we can define a fuzzy set denoted as *large*, and it corresponds to the membership function which is shown in Fig. 3.1. We see that we have to determine two important parameters *a* and *b*. The parameters *a* and *b* can be defined as

$$a(i, j)=mg(i, j) \tag{9}$$

$$b(i, j)=a(i, j)+0.2a(i, j) \tag{10}$$

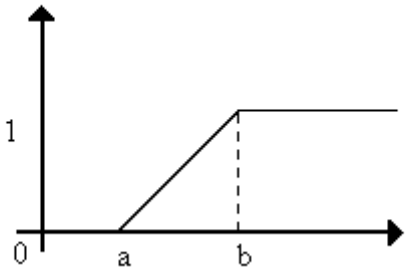

Fig. 3.1. The membership function corresponds to *large*.

Second, we consider a 3×3 neighborhood around the central pixel $I(i, j)$. Each of the eight neighbors of $I(i, j)$ corresponds to one direction {North West (*NW*), North (*N*), North East (*NE*), East (*E*), South East (*SE*), South (*S*), South West

(*SW*), West (*W*)} that is displayed in Fig. 3.2(a). We use the concept of the fuzzy gradient value which contains the basic gradient value and the related gradient value. The basic gradient value is donated as $\nabla_D I(i,j)$ of pixel position (i,j) in direction set D ($D \in \{NW, N, NE, W, E, SE, S, SW\}$). For example,

$$\nabla_{NW} I(i,j) = I(i-1, j-1) - I(i,j) \tag{11}$$

$$\nabla_{N} I(i,j) = I(i, j-1) - I(i,j) \tag{12}$$

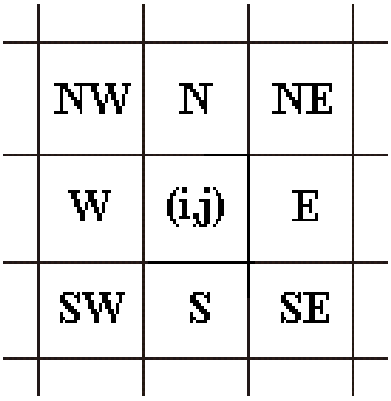

(a)

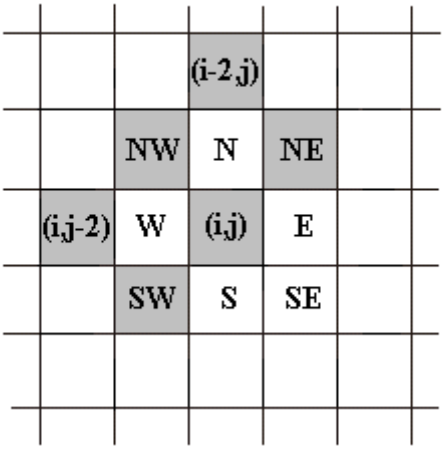

(b)

Fig. 3.2. (a) The neighborhood around the central pixel $I(i,j)$. (b) Pixel indicated in gray are used to compute the fuzzy gradient value of pixel $I(i,j)$ for *NW* direction.

TABLE 3.1
The fuzzy gradient in each direction

D	Basic gradient	Related gradient	Correspond direction
NW	$\nabla_{NW} I(i, j)$	$\nabla_{NW} I(i+1, j-1),\ \nabla_{NW} I(i-1, j+1)$	$SW-NE\ (45^\circ)$
N	$\nabla_{N} I(i, j)$	$\nabla_{N} I(i, j-1),\ \nabla_{N} I(i, j+1)$	$W-E\ (0^\circ)$
NE	$\nabla_{NE} I(i, j)$	$\nabla_{NE} I(i-1, j-1),\ \nabla_{NE} I(i+1, j+1)$	$SE-NW\ (135^\circ)$
W	$\nabla_{W} I(i, j)$	$\nabla_{W} I(i-1, j),\ \nabla_{W} I(i+1, j)$	$S-N\ (90^\circ)$
E	$\nabla_{E} I(i, j)$	$\nabla_{E} I(i-1, j),\ \nabla_{E} I(i+1, j)$	$S-N\ (90^\circ)$
SW	$\nabla_{SW} I(i, j)$	$\nabla_{SW} I(i-1, j-1),\ \nabla_{SW} I(i+1, j+1)$	$SE-NW\ (135^\circ)$
S	$\nabla_{S} I(i, j)$	$\nabla_{S} I(i, j-1),\ \nabla_{S} I(i, j+1)$	$W-E\ (0^\circ)$
SE	$\nabla_{SE} I(i, j)$	$\nabla_{SE} I(i-1, j+1),\ \nabla_{SE} I(i+1, j-1)$	$SW-NE\ (45^\circ)$

Next, we also calculate the related gradient value which corresponds to each of eight directions. For example, Fig. 3.2(b) shows the related gradient of the *NW* direction and it can be expressed as

$$\nabla'_{NW} I(i, j) = \nabla_{NW} I(i+1, j-1) = I(i, j-2) - I(i+1, j-1) \tag{13}$$

$$\nabla''_{NW} I(i, j) = \nabla_{NW} I(i-1, j+1) = I(i-2, j) - I(i-1, j+1) \tag{14}$$

In Table 3.1, we show a detail of the eight directions in the column 1, the basic gradient corresponds to each direction in column 2, the two related gradients correspond to each direction in column 3, and the correspond perpendicular direction in column 4. Actually, in the 3×3 window, the direction of the gradient only belong to $W-E$ direction (0°), $SW-NE$ direction (45°), $S-N$ direction (90°), and $SE-NW$ direction (135°). Thus, we can only compute the fuzzy gradient for the direction set ED where $ED \in \{NW, N, NE, W\}$ that contains all the orientations in the 3×3 window. For example, computing the fuzzy gradient for the *NW* direction and *SE*

direction are both equivalent to computing the gradient for the *SW*−*NE* direction (45°).

For each direction of the direction set *ED*, we calculate the fuzzy derivative donated as $\gamma_P(i,j)$ in each pixel (i,j) for direction *P*, where $P \in ED$. This is realized by the following fuzzy rule 1 :

Fuzzy Rules 1.

IF

$|\nabla_P I(i,j)|$ is *large* **AND** $|\nabla'_P I(i,j)|$ is *large* **AND** $|\nabla''_P I(i,j)|$ is *large*

OR

$|\nabla_P I(i,j)|$ is *large* **AND** $|\nabla'_P I(i,j)|$ is **not** *large* **AND** $|\nabla''_P I(i,j)|$ is *large*

OR

$|\nabla_P I(i,j)|$ is *large* **AND** $|\nabla'_P I(i,j)|$ is *large* **AND** $|\nabla''_P I(i,j)|$ is **not** *large*

THEN $\gamma_P(i,j)$ is *large* in direction *P*.

The **AND** operator (**OR** operator) can be the minimum (maximum) that are the well-known triangular norms (together with their dual co-norms) in the fuzzy logic. For the **not** operator, we use the standard negator $N(x)=1-x$ with $x \in [0,1]$. The *large* is the fuzzy set corresponds the membership function LARGE that was defined above. The idea of this rule is to consider an edge passing though the pixel $I(i,j)$ and its neighborhood for the direction, i.e. *SW*-*NE* direction (45°), not only the basic gradient value $|\nabla_P I(i,j)|$ will be large, but also the related gradient $|\nabla'_P I(i,j)|$ or $|\nabla''_P I(i,j)|$ can expect to be large. Therefore, if two out of three gradient values are small, it is safe to assume that no edge exists in the considered direction.

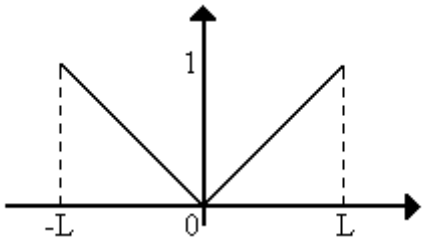

Fig. 3.3. The membership function corresponds to *absolute value*

Next, we again use a rule for each direction. The idea behind the rule is that if a pixel is assumed to be large in rule 1, then it probably can be consider as an edge for direction *P*, and the derivative value will be used to estimate the gradient direction of this pixel. Thus, we use the following rule 2 to compute $D^{P}_{gradient}$.

Fuzzy Rules 2.

IF

$\gamma_P(i,j)$ is *large* **AND** $\nabla_P I(i,j)$ is *absolute value*

THEN $D^{P}_{gradient}$ is *absolute value* in direction *P*.

where the fuzzy set *absolute value* corresponds to the membership function which is shown as Fig. 3.3 and the parameter $L = 255$ is used in the experiment. The **AND** operator is also the minimum in the fuzzy logic.

The final step in the computation of the fuzzy gradient is the defuzzification. We are interested in obtaining the direction that has maximum value of $D^{P}_{gradient}$. P^*, which is estimated to be the gradient direction in pixel (i,j), is determined by

$$P^* = \arg\max_{P \in ED} D^{P}_{gradient} I(i,j) \qquad (15)$$

Finally, we rotate the window with the angle that corresponds to P^*. For using the adjustable window, the VMD method will be more robust for detecting the edge

response. The experiment will be discussed in Chapter 4.

3.2 Automatic Threshold Selection

To automatically obtain the best threshold that is adaptive to the image contents, we propose a new method for hysteresis thresholding method combining the merits of Yitzhaky and Peli [17] and Medina *et al.* [18] methods. Yitzhaky and Peli can find the best thresholds within a set of possible values, but the performance will depend on the set of possible values choosen. On the other hand Medina *et al.* method is similar to Yitzhaky and Peli, but the performance will depend on one's choice of the subset and the overset. In the following, we will introduce how to apply the thresholding methods to VMD method.

3.2.1 Determine Parameter Set

Fig. 3.3 shows the symbolic graphic of the choice of parameter set. For an image *I*, let E_I be the unknown true edge points set of the image *I* with the condition $A_I \subseteq E_I \subseteq B_I$ where A_I and B_I are the subset and the overset of the image *I*. For a possible hysteresis thresholds set *C*, for example

$$C = \left\{ (t_{low}, t_{high}) \;\middle|\; t_{low}, t_{high} \in [0,\ 1],\ t_{low} < t_{high} \right\}$$

we want to find the parameter set *T* in the region between the subset A_I and the overset B_I. Thus, we will get the best edge map $E_{t_{low}, t_{high}}$ determined by hysteresis thresholds t_{low} and t_{high} with $(t_{low}, t_{high}) \in T$ in the next section.

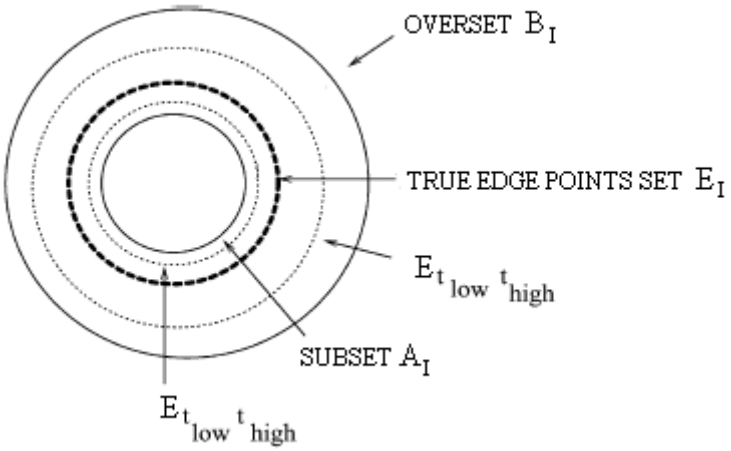

Fig. 3.3. The symbolic graphic of the choice of parameter set [18].

Considering the feature image histogram is usually unimodal, we use the Otsu method [11] and the Rosin method [12] to determine the subset A_I and the overset B_I. The Otsu method is not very sensitive on unimodal histograms and performs rigorously on detecting edge points for edge detection, but edge pixels detected by the Otsu method have a high probability of being true edge points. Thus, the edge map E_{Otsu} can be utilized as the subset of the image. The Rosin method is very sensitive on unimodal histograms and it can be noisy for edge detection, but the Rosin method can usually detect the true edge pixels together with many fakery ones. Thus, the edge map $E_{Ro\sin}$ can be employed as the overset of the image. If the conditions $E_{t_{low},t_{high}} \subseteq E_{Ro\sin}$ and $E_{Ostu} \subseteq E_{t_{low},t_{high}}$ hold, then the following expression can easily be proved

$$FP(E_{t_{low},t_{high}}, E_{Ro\sin}) = 0$$

$$FN(E_{t_{low},t_{high}}, E_{Ostu}) = 0 \qquad (16)$$

where *FP* and *FN* are False Positive and False Negative in ROC analysis [19]. Here, *FP* indicates that the points were decided as edges in $E_{t_{low},t_{high}}$ and coincide with

non-edge points in $E_{Ro\sin}$. FN indicates that the points were decided as non-edges in $E_{t_{low},t_{high}}$ and coincide with edge points in E_{Ostu}.

Actually, there is some error probability may exist between E_{Otsu} and $E_{Ro\sin}$ such that we can not find any hysteresis thresholds t_{low} and t_{high} with $(t_{low},t_{high}) \in C$ and satisfing $FP(E_{t_{low},t_{high}},E_{Ro\sin}) = 0$ and $FN(E_{t_{low},t_{high}},E_{Ostu}) = 0$. For this case, we can consider whether the following expressions are true or not.

$$FN(E_{t_{low},t_{high}},E_{Ro\sin}) \neq 0$$

$$FP(E_{t_{low},t_{high}},E_{Ostu}) \neq 0 \qquad (17)$$

$FN(E_{t_{low},t_{high}},E_{Ro\sin}) \neq 0$ implies that there are negatives in the edge map $E_{t_{low},t_{high}}$ that are positives in the set $E_{Ro\sin}$, and $FP(E_{t_{low},t_{high}},E_{Ostu}) \neq 0$ implies that there are positives in the edge map $E_{t_{low},t_{high}}$ that are negatives in the set E_{Otsu}. Thus, let C_H and C_K be the sets that define as

$$C_H = \left\{ (t_{low},t_{high}) \;\middle|\; t_{low},t_{high} \in C \right\} \text{ with the condition (16)}$$

$$C_K = \left\{ (t_{low},t_{high}) \;\middle|\; t_{low},t_{high} \in C \right\} \text{ with the condition (17)}$$

The parameter set *T* can be determined by

If $C_H \neq \Phi$

Then the parameter set $T = C_H$

Else if $C_K \neq \Phi$

Then the parameter set $T = C_K$

Else

Then the parameter set $T = C$

3.2.2 The Best Threshold Selection

Here, we will find the best hysteresis thresholds within the parameter set T determined above. For a parameter set T, in the first, we can construct an image map PGT (potential ground truth) using all edge maps $E_{t_{low},t_{high}}$ that determined by the hysteresis thresholds with $(t_{low},t_{high}) \in T$. Defining an edge pixel as "1" and a non-edge pixel as "0" for all edge maps $E_{t_{low},t_{high}}$, each pixel of the PGT image will get a value from the sum of the correspond pixel of all edge maps $E_{t_{low},t_{high}}$. For example, consider a pixel $p \in I$, there are q different edge maps $E_{t_{low},t_{high}}$ with different hysteresis thresholds t_{low} and t_{high}, where $(t_{low},t_{high}) \in T$, detect the pixel p as an edge pixel, then we mark the value of q to this pixel in the PGT image. It means that there are q hysteresis threshold sets support the pixel p to be an edge.

Second, we will compute the maximum value of the PGT image. If the maximum value is L, then the PGT_i can be obtained by threshold the PGT image with possible thresholds $i = 0, 1, ..., L-1$. For each PGT_i edge map, we calculate *TP*, *TN*, *FP* and *FN* that indicate True Positive, True Negative, False Positive and False Negative from comparing with each $E_{t_{low},t_{high}}$, and the average of all the probabilities resulting are computed by

$$\overline{TP_{PGT_i}} = \frac{1}{N} \sum_{(t_{low},t_{high} \in T)} TP_{PGT_i,E_{t_{low},t_{high}}} \quad \text{with} \quad i = 0,\ 1,\ ...,\ L-1 \tag{18}$$

$$\overline{TN_{PGT_i}} = \frac{1}{N} \sum_{(t_{low},t_{high} \in T)} TN_{PGT_i,E_{t_{low},t_{high}}} \quad \text{with} \quad i = 0,\ 1,\ ...,\ L-1 \tag{19}$$

$$\overline{FP_{PGT_i}} = \frac{1}{N} \sum_{(t_{low}, t_{high} \in T)} FP_{PGT_i, E_{t_{low}, t_{high}}} \quad \text{with} \quad i = 0,\ 1,\ ...,\ L-1 \tag{20}$$

$$\overline{FN_{PGT_i}} = \frac{1}{N} \sum_{(t_{low}, t_{high} \in T)} FN_{PGT_i, E_{t_{low}, t_{high}}} \quad \text{with} \quad i = 0,\ 1,\ ...,\ L-1 \tag{21}$$

where $TP_{PGT_i, E_{t_{low}, t_{high}}}$ indicates the pixels are edges in the PGT_i and coincide with edges in the $E_{t_{low}, t_{high}}$. $TN_{PGT_i, E_{t_{low}, t_{high}}}$ indicates the pixels are non-edges in the PGT_i and coincide with non-edges in the $E_{t_{low}, t_{high}}$. $FP_{PGT_i, E_{t_{low}, t_{high}}}$ indicates the pixels are edges in the PGT_i but detected as non-edges in the $E_{t_{low}, t_{high}}$. $FN_{PGT_i, E_{t_{low}, t_{high}}}$ indicates the pixels are non-edges in the PGT_i but detected as edges in the $E_{t_{low}, t_{high}}$. N represents the cardinality of the parameter set T. Next, the Chi-square test of the optimal threshold can be calculated by

$$\chi^2_{PGT_i} = \frac{\overline{Sn_{PGT_i}} - Q_{PGT_i}}{1 - Q_{PGT_i}} \frac{\overline{Sp_{PGT_i}} - (1 - Q_{PGT_i})}{Q_{PGT_i}} \tag{22}$$

where

$$Q_{PGT_i} = \overline{TP_{PGT_i}} + \overline{FP_{PGT_i}}$$

$$\overline{Sn_{PGT_i}} = \frac{\overline{TP_{PGT_i}}}{\overline{TP_{PGT_i}} + \overline{FN_{PGT_i}}}$$

$$\overline{Sp_{PGT_i}} = \frac{\overline{TN_{PGT_i}}}{\overline{TN_{PGT_i}} + \overline{FP_{PGT_i}}}$$

Finally, a higher $\chi^2_{PGT_i}$ can obtain a better threshold. The best threshold in parameter set T is correspond to the value of i that maximizes $\chi^2_{PGT_i}$. Thus, we have the following conclusion: If $k = \arg\max_{i \in \{0,1,...,L-1\}} \chi^2_{PGT_i}$, then the hysteresis thresholds

$\left(t^*_{tlow}, t^*_{thigh}\right) = \arg\max_{(t_{low},t_{high})\in T} \mu\left(E_{t_{low},t_{high}}\right)$ will be the best choice, where

$$\mu\left(E_{t_{low},t_{high}}\right)$$

$$= \chi^2_{E_{t_{low},t_{high}},PGT_k}$$

$$= \frac{Sn^*_{PGT_k,E_{t_{low},t_{high}}} - Q^*_{PGT_k,E_{t_{low},t_{high}}}}{1-Q^*_{PGT_k,E_{t_{low},t_{high}}}} \frac{Sp^*_{PGT_k,E_{t_{low},t_{high}}} - \left(1-Q^*_{PGT_k,E_{t_{low},t_{high}}}\right)}{Q^*_{PGT_k,E_{t_{low},t_{high}}}} \quad (23)$$

and

$$Q^*_{PGT_k,E_{t_{low},t_{high}}} = TP_{PGT_k,E_{t_{low},t_{high}}} + FP_{PGT_k,E_{t_{low},t_{high}}}$$

$$Sn^*_{PGT_k,E_{t_{low},t_{high}}} = \frac{TP_{PGT_k,E_{t_{low},t_{high}}}}{TP_{PGT_k,E_{t_{low},t_{high}}} + FN_{PGT_k,E_{t_{low},t_{high}}}}$$

$$Sp^*_{PGT_k,E_{t_{low},t_{high}}} = \frac{TN_{PGT_k,E_{t_{low},t_{high}}}}{TN_{PGT_k,E_{t_{low},t_{high}}} + FP_{PGT_k,E_{t_{low},t_{high}}}}$$

One of the drawbacks of Yitzhaky and Peli method is that the result depends on the parameter set we choose. For different parameter sets, very different results will be obtained. Thus, after the improvement of the choice of the parameter set, a more reliable result will be obtained.

Chapter 4 Experimental Results

In Chapter 4, we compare our method with the original VMD detector on simple synthetic images in Section 4.1. In Section 4.2, the synthetic color images are generated for assessing the performance comparison with different automatic thresholding techniques. In the end of this chapter, for comparison, the compass operator of Ruzon and Tomasi [7], Canny edge detector [1], RCMG detector [9], and MVD edge detector [4] are used. We evaluate the edge detection techniques quantitatively by using Pratt's Figure of Merit (FOM) [20] and Receiver Operating Characteristic (ROC) analysis [19].

4.1 Comparison with the Original VMD Detector

We mentioned that VMD detector has weak ability for detecting oblique edges in Section 3.1, and for improving the drawbacks of the VMD detector, we also proposed the method that adjusted the orientation of window according to the direction of the gradient which was derived from the fuzzy gradient method.

To verify our approach is useful for VMD detector, some simple tests are shown as Figs. 4.1 – 4.5. As shown in Figs. 4.1 – 4.5, we treat these test images for partitioning into white, black, and gray regions, and the edges for different directions are salient. Examining the edge strength as scale value from the original VMD detector and the improved VMD detector, the results are plotted. Fig. 4.1 and Fig. 4.2 show the test images with the salient edges for 0° and 90° of the edge directions, respectively. We can see the edge responses of the original VMD detector and the improved VMD detector are similar in Figs. 4.1(b) – (c), and Figs. 4.2(b) – (c) show that the edge response of the original VMD detector becomes blunter than the edge

(a)

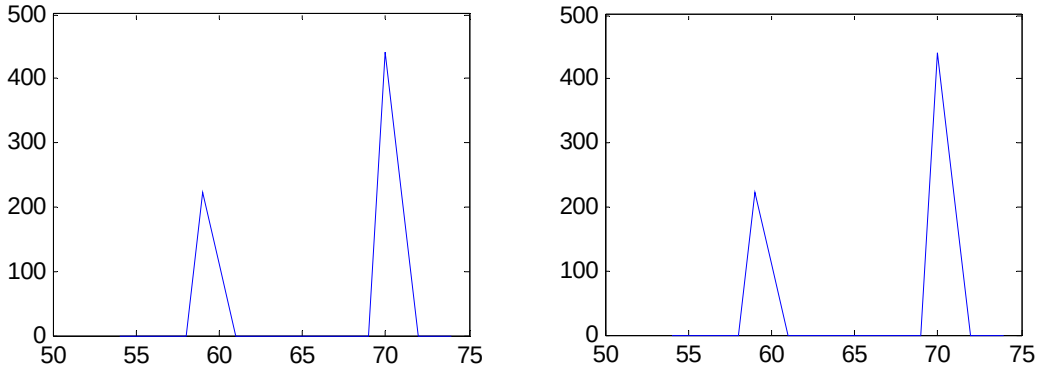

(b) (c)

Fig. 4.1. Comparison of the edge response for 0° edges. (a) The test image. (b) The edge response of the original VMD detector. (c) The edge response of the improved VMD detector.

response of the improved VMD detector. Also the ideal edges for 45° and 135° of the edge directions shown as Fig. 4.3(a) and Fig. 4.4(a), respectively, both the edge responses of the original VMD detector are less distinguishable in the Figs. 4.3(b)−(c)and Figs. 4.4(b)−(c). An oblique edge for the arbitrary direction is shown as Fig. 4.5(a). For Figs. 4.5(b)−(c), the original VMD detector produce three peaks such that a worse edge map may occur with wrong edges.

However, a strong and sharp response is much distinguishable for edge detection. The proposed improved VMD detector can maintain the shaper response for different edge directions. These experiments show that the propose method is more robust and

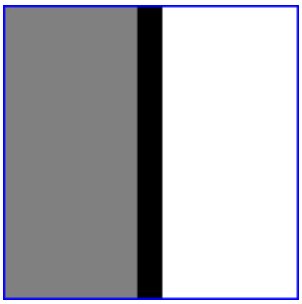

(a)

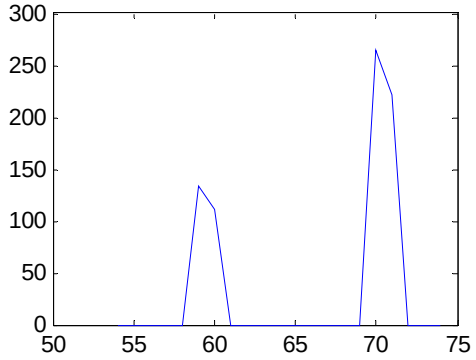

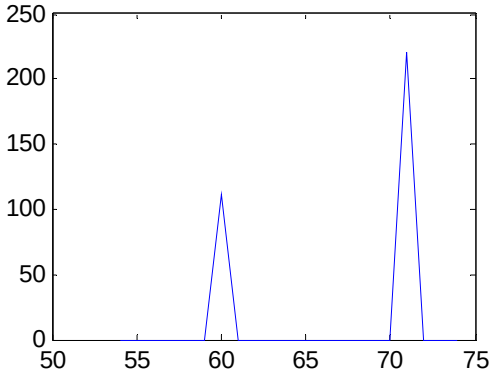

(b) (c)

Fig. 4.2. Comparison of the edge response for 90° edges. (a) The test image. (b) The edge response of the original VMD detector. (c) The edge response of the improved VMD detector.

reliable.

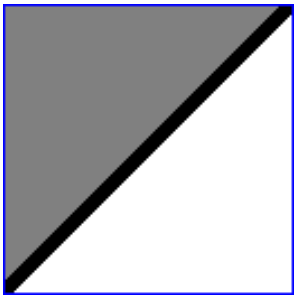

(a)

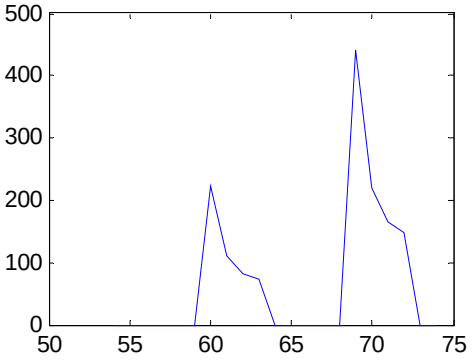

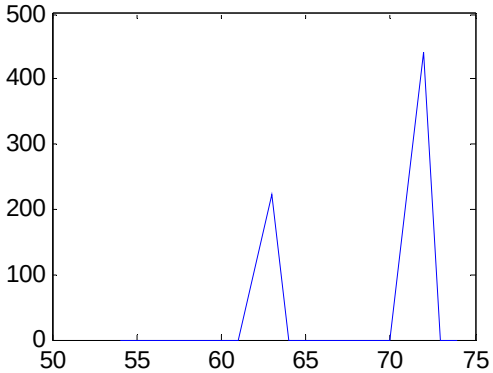

(b) (c)

Fig. 4.3. Comparison of the edge response for 45° edges. (a) The test image. (b) The edge response of the original VMD detector. (c) The edge response of the improved VMD detector.

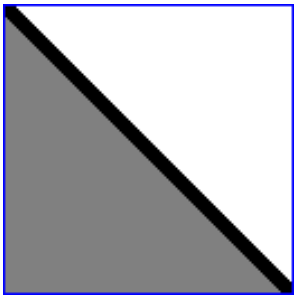

(a)

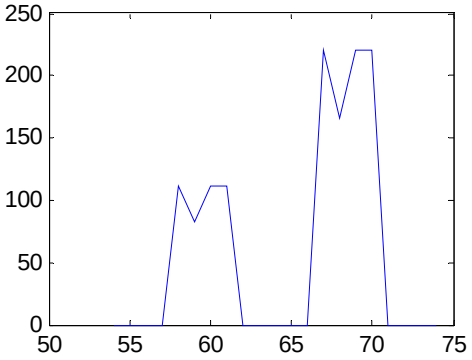

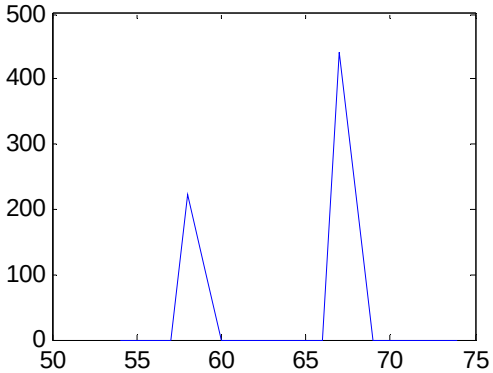

(b) (c)

Fig. 4.4. Comparison of the edge response for 135° edges. (a) The test image. (b) The edge response of the original VMD detector. (c) The edge response of the improved VMD detector.

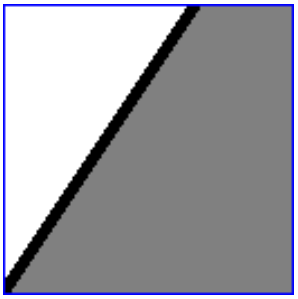

(a)

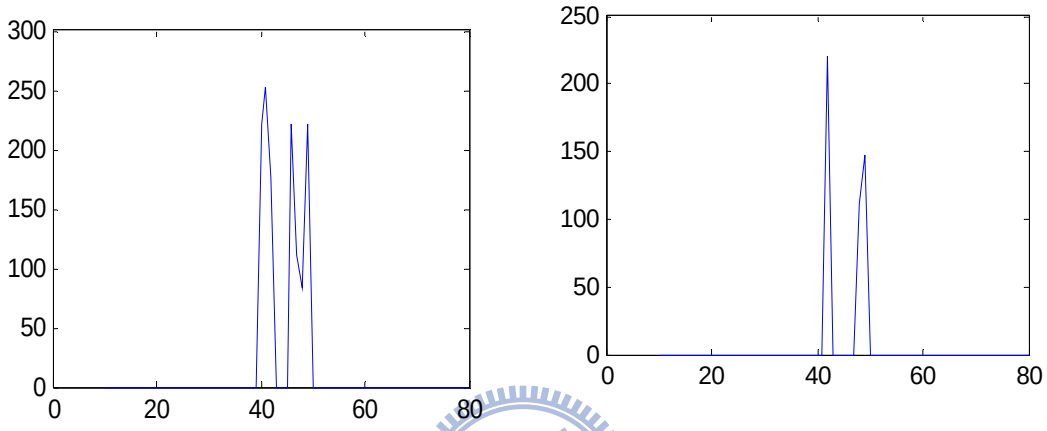

(b) (c)

Fig. 4.5. Comparison of the edge response for an oblique edge with the arbitrary direction. (a) The test image. (b) The edge response of the original VMD detector. (c) The edge response of the improved VMD detector.

4.2 Comparison with Different Automatic Thresholding Techniques

4.2.1 Quantitative Evaluation

The evaluations of edge detectors are usually subjective by observers [21]. Most of the objective evaluation methods assume that the specific features of images are known such as boundaries in simple synthetic images. In such cases, for the known ideal edges considered to be the ground truth (GT), the quantitative of the edge detection can be measured. In nature images, Bowyer [22] manually created specification of the edges to form a GT, and Fernandez [23] used an automatic statistical method to generate GT images. However, for a quantitative evaluation, different criteria will produce different result. The approach adopted here is to use the GT images generated from synthetic image with the widely used performance measures, FOM [20] and ROC analysis [19].

First, The FOM is defined by

$$FOM = \frac{1}{\max\{I_D, I_I\}} \sum_{i=1}^{I_D} \frac{1}{1+\alpha(d_i)^2} \times 100\% \tag{24}$$

where I_D and I_I are the number of detected and number of ideal edge points respectively, α (>0) is a calibration constant, and d_i is the edge deviation for the *i*-th detected edge pixel. In all cases $0 < \text{FOM} \leq 1$; for a perfect match between the detected and the ideal edges $\text{FOM} = 1$ whereas the detected edges deviate more and more from the ideal ones FOM goes to zero. The scaling constant $\alpha = 0.2$ proposed in [9] has been adopted.

Next, we would like to introduce the True Positive Rate (TPR), True Negative Rate (TNR) and Normalized Accuracy (NACC) of ROC analysis. The TPR is defined by

$$TPR = \frac{TP}{(TP + FN)} \times 100\% \tag{25}$$

where TP represents the number of pixels which are detected as an edge pixel and belong to an ideal edge pixel, and FN represents the number of pixels which are detected as an edge pixel but belong to an ideal non-edge pixel. On the other hand, the TNR is defined as

$$TNR = \frac{TN}{TN + FP} \times 100\% \tag{26}$$

where TN represents the number of pixels which are detected as an non-edge pixel and belong to an ideal non-edge pixel, and FP represents the number of pixels which are detected as an non-edge pixel but belong to an ideal edge pixel. Finally, we calculate the normalized accuracy (NACC) by

$$NACC = \frac{TPR + TNR}{2} \times 100\% \tag{27}$$

NACC = 100% corresponds to a perfect match between the ideal edge and detected edge points and as the deviation of the edge points increase, the NACC approaches to zero percentage.

4.2.2 Edge Results of Different Threshold Methods in Synthetic Color Images

In this experiment, eleven 128×128 and eleven 256×256 synthetic color images were used. The 128×128 and 256×256 synthetic images individually have the same form with different color components. We compared the performance of the improved VMD detector, where thresholds were determine by Yitzhaky and Peli method [17], Medina *et al.* method [18], and our thresholding method, respectively. In Figs. 4.6 – 4.9, we show some of the edge detection results of the synthetic color images for

(a)

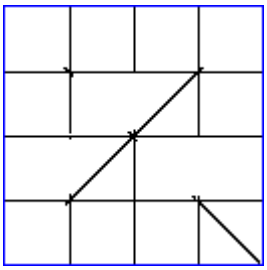

(b)

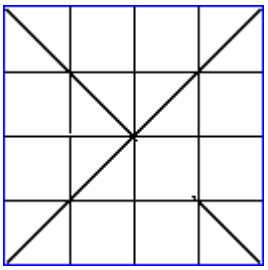

(c)

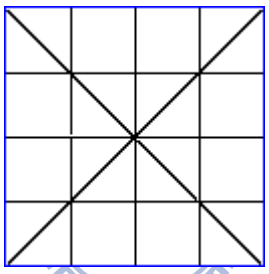

(d)

Fig. 4.6. Edge detection results of the 128×128 synthetic image Sample 1 detected by the improved VMD detector, where the thresholds are determined by different methods. (a) Original image. (b) Thesholding by Yitzhaky and Peli method. (c) Thesholding by Medina *et al.* method. (d) Thesholding by our method.

comparison. For Figs. 4.6(b)–(d), the edge map thresholding by our method detects more true edges than the other two thresholding method. Fig. 4.7(b) represents the edge map thresholding by Yitzhaky and Peli method is less sensitive than the other two shown as Figs. 4.7(c) and (d). In 256×256 synthetic images, our thresholding method also gets more robust results when the color components vary in Figs. 4.8 and 4.9.

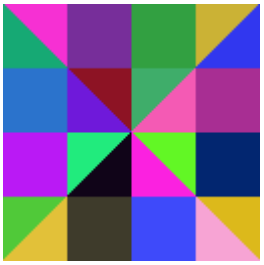

(a)

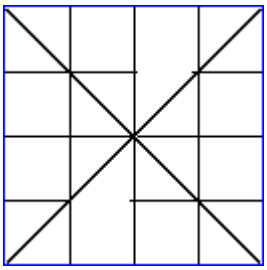

(b)

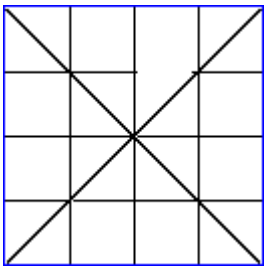

(c)

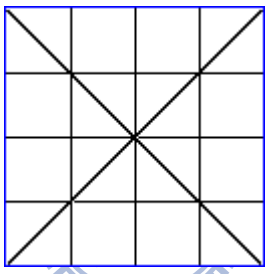

(d)

Fig. 4.7. Edge detection results of the 128×128 synthetic image Sample 2 detected by the improved VMD detector, where the thresholds are determined by different methods. (a) Original image. (b) Thesholding by Yitzhaky and Peli method. (c) Thesholding by Medina *et al.* method. (d) Thesholding by our method.

Tables 4.1, 4.2 and 4.3 show the average performances of the eleven 128×128, 256×256 synthetic images and the total images detected by the improved VMD detector with various thresholding methods which is shown in the order of column 1. The column 2 to column 5 shows the value of FOM, TPR, TNR, and NACC, respectively. From Tables 4.1 – 4.3, we can see that our thresholding method performs well than the others.

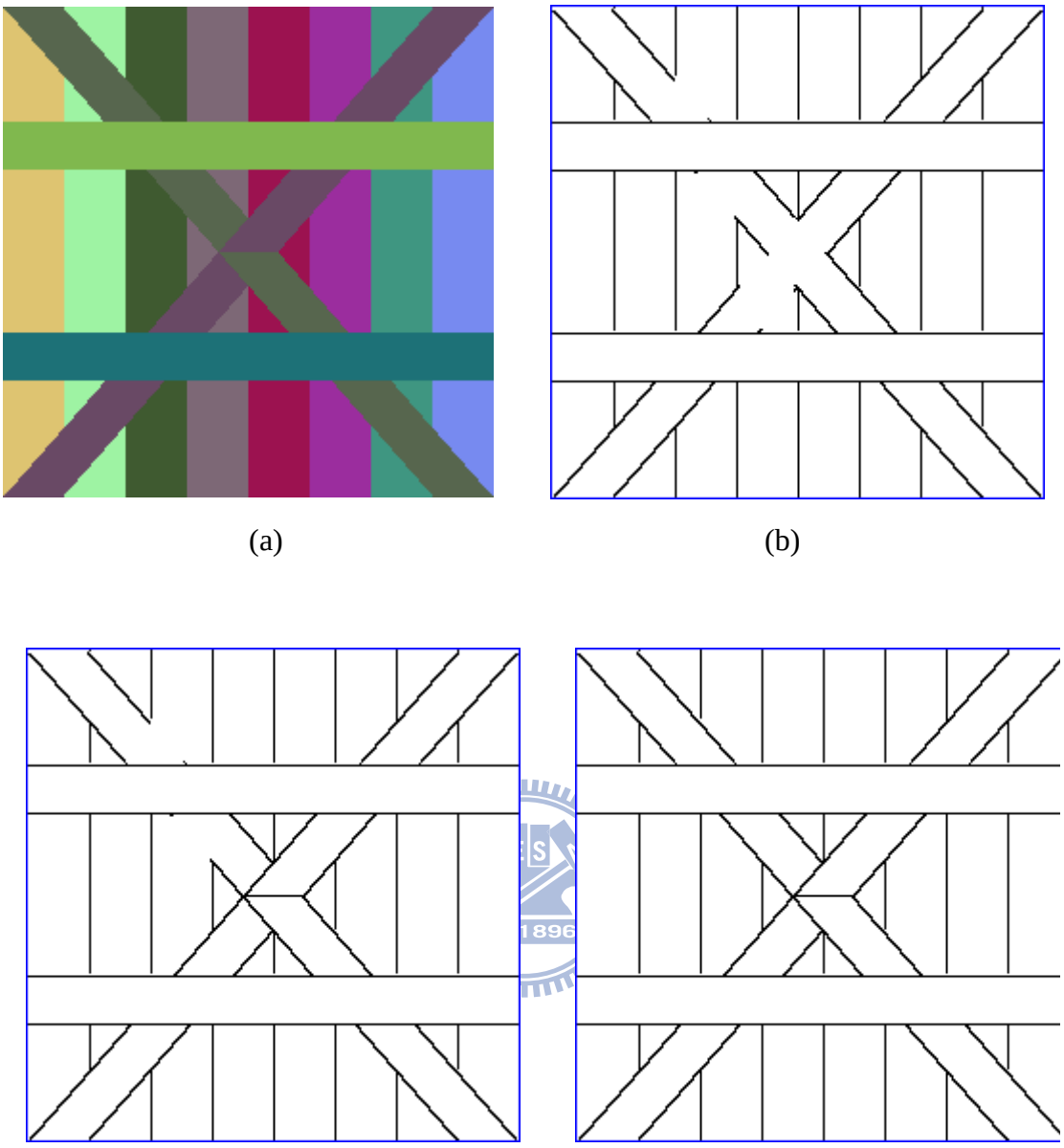

(a) (b)

(c) (d)

Fig. 4.8. Edge detection results of the 256×256 synthetic image Sample 3 detected by the improved VMD detector, where the thresholds are determined by different methods. (a) Original image. (b) Thesholding by Yitzhaky and Peli method. (c) Thesholding by Medina *et al.* method. (d) Thesholding by our method.

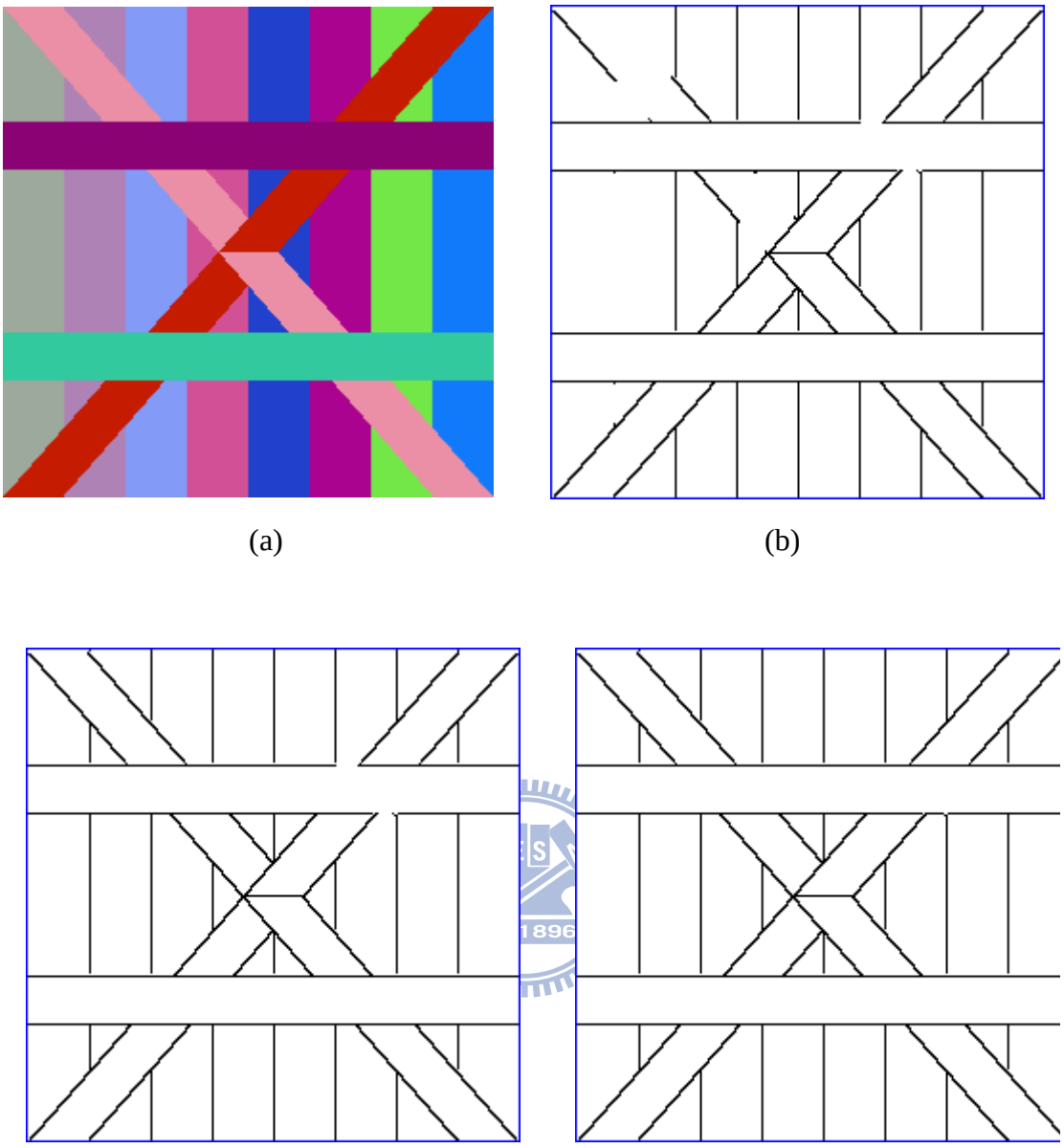

(a) (b)

(c) (d)

Fig. 4.9. Edge detection results of the 256×256 synthetic image Sample 4 detected by the improved VMD detector, where the thresholds are determined by different methods. (a) Original image. (b) Thesholding by Yitzhaky and Peli method. (c) Thesholding by Medina *et al.* method. (d) Thesholding by our method.

TABLE 4.1
The average evaluation results of the eleven 128×128 synthetic color images detected by the improved VMD detector with the following thresholding methods

Thresholding Method	FOM (%)	TPR (%)	TNR (%)	NACC (%)
Yitzhaky and Peli	89.84_3	99.98	99.17	99.58_3
Medina *et al.*	96.86_2	99.98	99.74	99.86_2
Our method	99.54_1	99.98	99.96	99.97_1

TABLE 4.2
The average evaluation results of the eleven 256×256 synthetic color images detected by the improved VMD detector with the following thresholding methods

Thresholding Method	FOM (%)	TPR (%)	TNR (%)	NACC (%)
Yitzhaky and Peli	93.55_3	99.96	99.63	99.80_3
Medina *et al.*	96.98_2	99.96	99.83	99.90_2
Our method	99.40_1	99.96	99.96	99.96_1

TABLE 4.3
The average evaluation results of the total synthetic color images detected by the improved VMD detector with the following thresholding methods

Thresholding Method	FOM (%)	TPR (%)	TNR (%)	NACC (%)
Yitzhaky and Peli	91.70_3	99.97	99.40	99.69_3
Medina *et al.*	96.92_2	99.97	99.78	99.88_2
Our method	99.47_1	99.97	99.96	99.97_1

4.2.3 Edge Results of Different Threshold Methods in Nature Color Images

In nature color images, the subjective performance of the edge detection remains a fundamental component of results interpretation. Figs. 4.10 and 4.11 show the

(a)

(b) (c)

(d)

Fig. 4.10. Edge detection results of the Peppers image detected by the improved VMD detector, where the thresholds are determined by different methods. (a) Original image. (b) Thesholding by Yitzhaky and Peli method. (c) Thesholding by Medina *et al.* method. (d) Thesholding by our method.

(a)

(b) (c)

(d)

Fig. 4.11. Edge detection results of the Lena image detected by the improved VMD detector, where the thresholds are determined by different methods. (a) Original image. (b) Thesholding by Yitzhaky and Peli method. (c) Thesholding by Medina *et al.* method. (d) Thesholding by our method.

Peppers and Lena images for comparison. The Medina *et al.* method supplies the most sensitive result within three thresholding methods in comparison, but it also detect more noise. The Yitzhaky and Peli method performs most rigorously and miss some edges that really exist in the image. In comparison, our thresholding method not only detects more true edges than the Yitzhaky and Peli method but also be less noisy than the Medina *et al.* method.

4.3 Comparison with Other Color Edge Detector

4.3.1 Quantitative Evaluation in Synthetic Color Images

Canny [1] presented the very popular aspects that good edge detection must not miss the true edge nor detect non-edge points as the edge points and produce thin and continuous lines. For these criteria, we also use the eleven 128×128 and eleven 256×256 synthetic color images for quantitative evaluation of the color edge detectors. The performances of our automatic color edge detection techniques are compared to those by the compass operator of Ruzon and Tomasi [7], Canny edge detector [1], RCMG detector [9], and MVD edge detector [4].

Fig. 4.12 show the edge detection results of 128×128 synthetic images for comparison. For the Fig. 4.12(b), using the parameter $\sigma = 0.94$, the figure is obtained by subjectively adjust the hysteresis thresholds for the compass operator with nonmaximal suppression (NMS). In contrast with Fig. 4.12(b), Fig. 4.12(c) shows the result that we adopted the Medina *et al.* thresolding method for the compass operator with NMS. We can see that both the result in Figs. 4.12(b) and (c) detect much noise in the regions near the corners. Setting the parameters to $k = 2$ and $l = 4$, the problem in Fig. 4.12(d), which is obtained by MVD detector, is that it has thicker

(a)

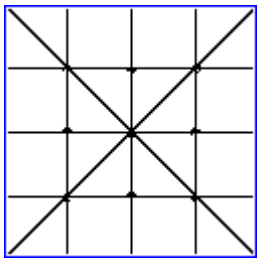

(b)

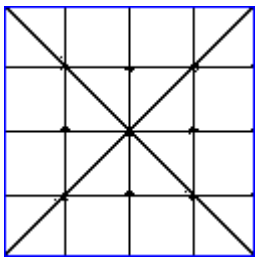

(c)

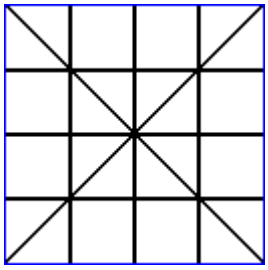

(d)

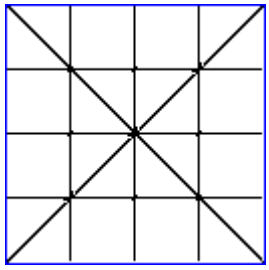

(e)

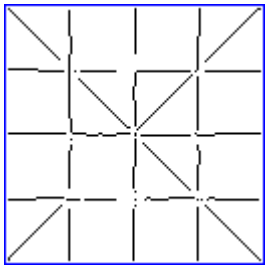

(f)

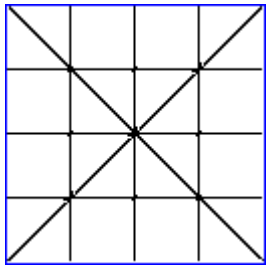

(g)

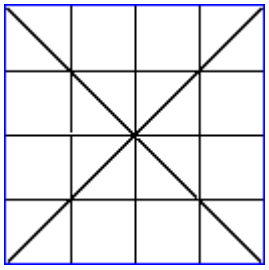

(h)

Fig. 4.12. Edge detection results of the 128×128 synthetic image Sample 1 detected by different color edge detectors. (a) Original image. (b) Compass result, (c) The compass operator with NMS and thresholding by Medina *et al.* method. (d) MVD result. (e) MVD with thinning process and thresholding by Medina *et al.* method. (f) Color Canny result. (g) RCMG with thinning process and thresholding by Medina *et al.* method. (h) Our automatic color edge detector.

responses for every edge point. Therefore, the thinning process is applied to MVD detector, and we also use the Medina *et al.* method for the edge detection and shown as Fig. 4.12(e). To apply Canny detector to color images, a method named Color Canny individually use Canny detector to detect edges for three dimensions in the color space, and determine the edge result by the majority vote fusion rule. In the edge result detected by Color Canny detector, which is shown in Fig. 4.12(f), the continuity of the edges perform worse than the others, especially in the corners. Fig. 4.12(g) shows the result detected by RCMG with the parameter $s = 1$ in the 3×3 window . Fig. 4.12(h) shows the result with our method, and it detects less noise and produce continuous lines for edge detection. More results are shown in Figs. 4.13 – 4.15. In Fig. 4.13(c), some ideal edges are missed by the compass operator thresholding by Medina *et al.* method.

(a)

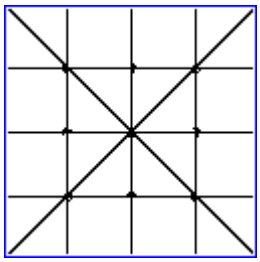

(b)

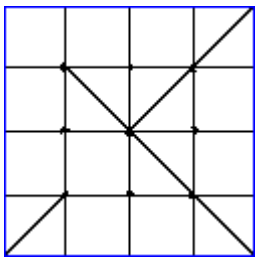

(c)

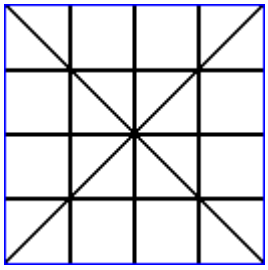

(d)

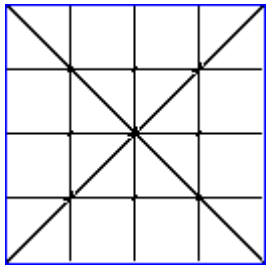

(e)

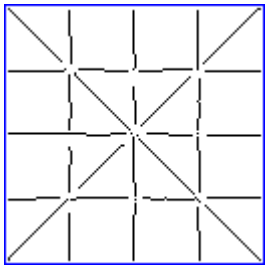

(f)

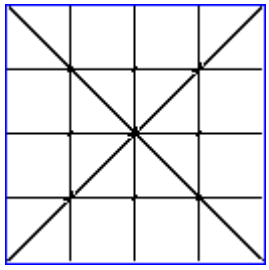

(g)

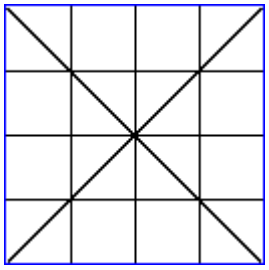

(h)

Fig. 4.13. Edge detection results of the 128×128 synthetic image Sample 2 detected by different color edge detectors. (a) Original image. (b) Compass result, (c) The compass operator with NMS and thresholding by Medina *et al.* method. (d) MVD result. (e) MVD with thinning process and thresholding by Medina *et al.* method. (f) Color Canny result. (g) RCMG with thinning process and thresholding by Medina *et al.* method. (h) Our automatic color edge detector.

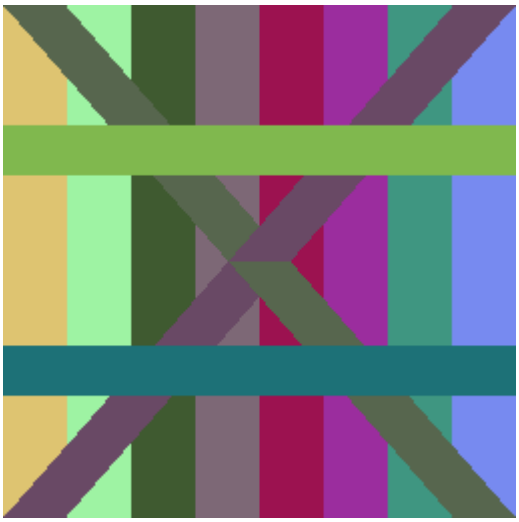

(a)

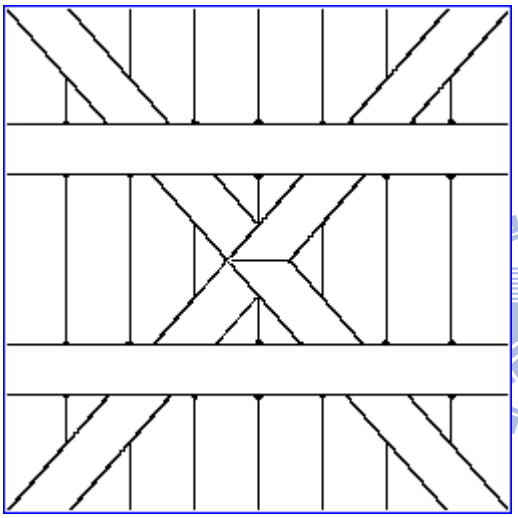

(b)

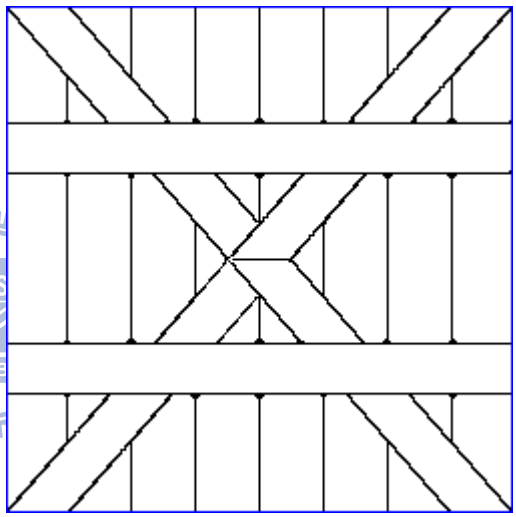

(c)

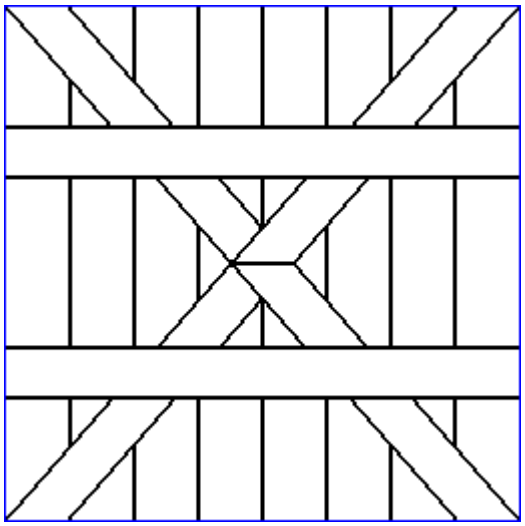

(d)

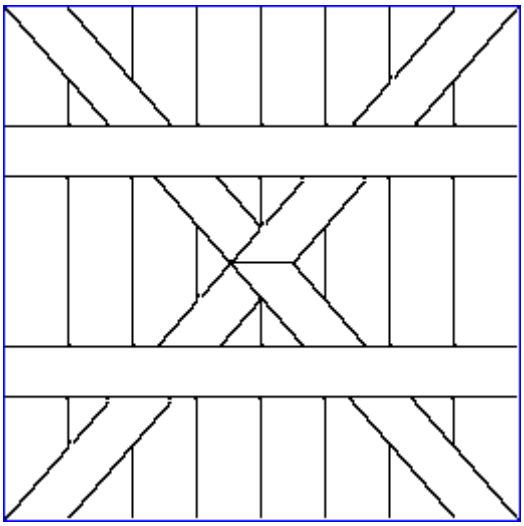

(e)

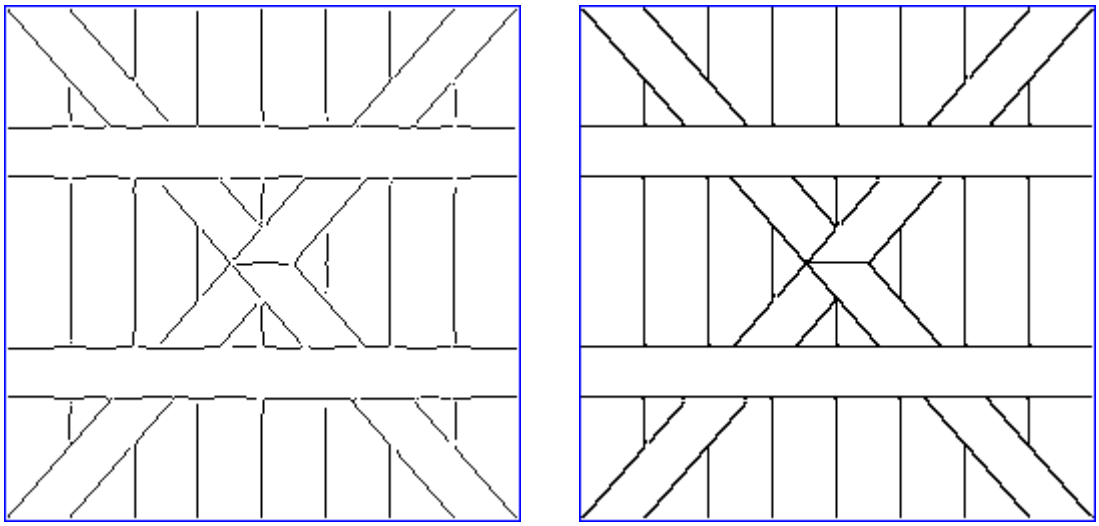

(f) (g)

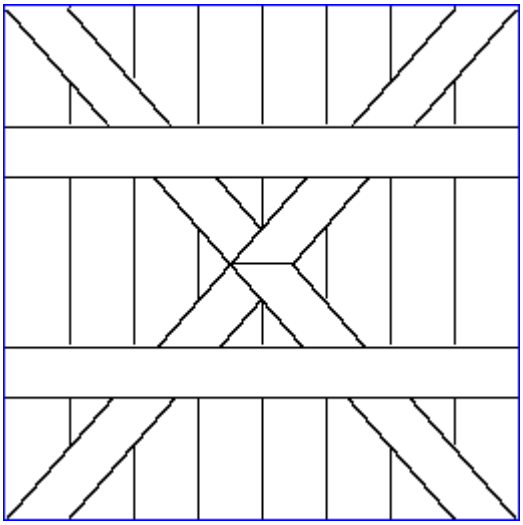

(h)

Fig. 4.14. Edge detection results of the 256×256 synthetic image Sample 3 detected by different color edge detectors. (a) Original image. (b) Compass result, (c) The compass operator with NMS and thresholding by Medina *et al.* method. (d) MVD result. (e) MVD with thinning process and thresholding by Medina *et al.* method. (f) Color Canny result. (g) RCMG with thinning process and thresholding by Medina *et al.* method. (h) Our automatic color edge detector.

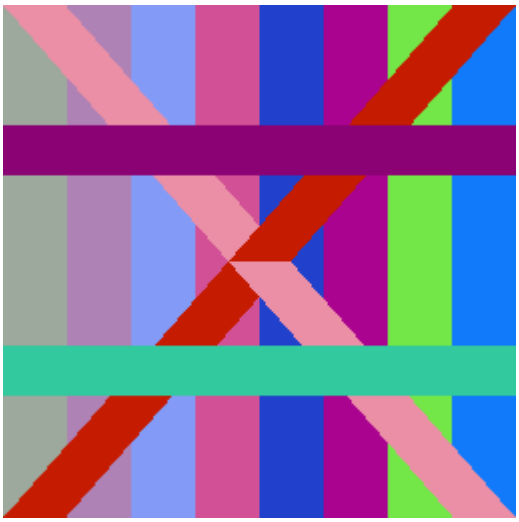

(a)

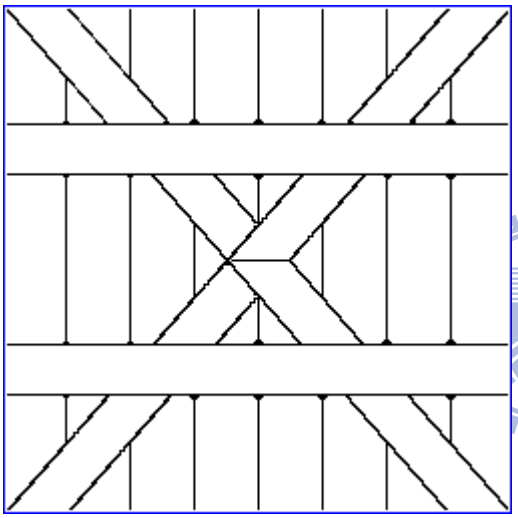

(b)

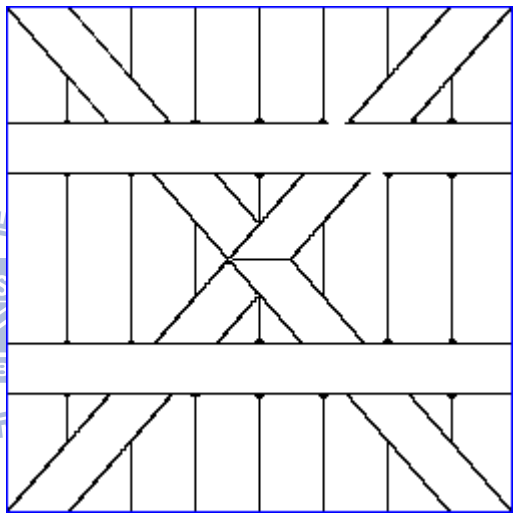

(c)

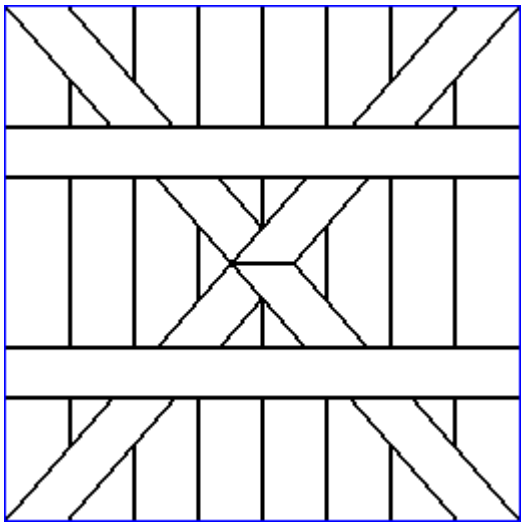

(d)

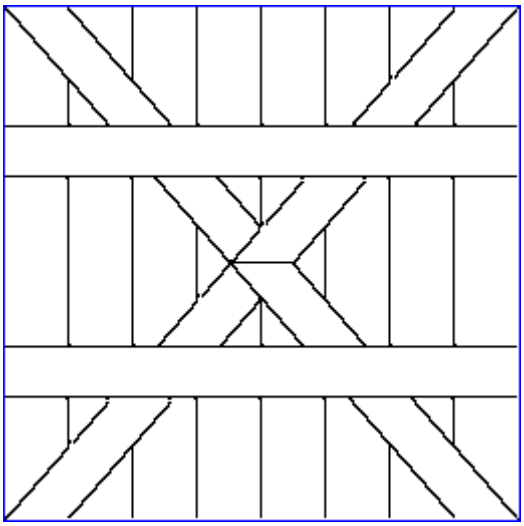

(e)

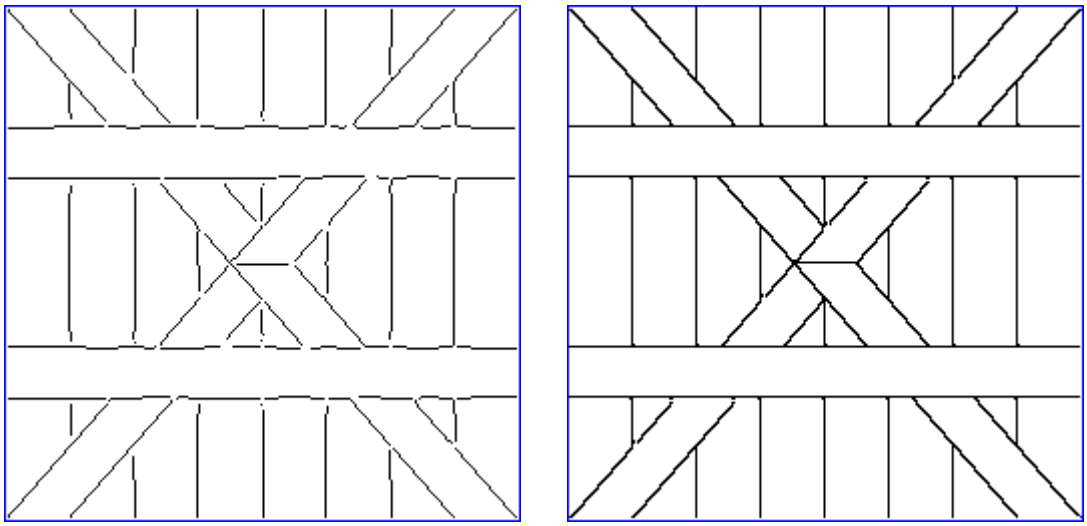

(f) (g)

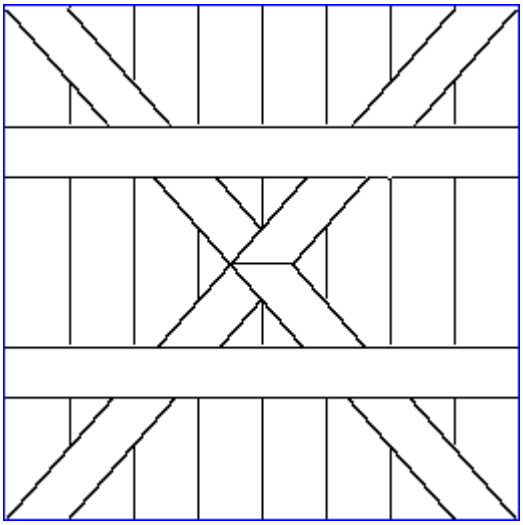

(h)

Fig. 4.15. Edge detection results of the 256×256 synthetic image Sample 4 detected by different color edge detectors. (a) Original image. (b) Compass result, (c) The compass operator with NMS and thresholding by Medina *et al.* method. (d) MVD result. (e) MVD with thinning process and thresholding by Medina *et al.* method. (f) Color Canny result. (g) RCMG with thinning process and thresholding by Medina *et al.* method. (h) Our automatic color edge detector.

Tables 4.4, 4.5 and 4.6 show the average performances of the eleven 128×128, 256×256 synthetic images and the total images for the compared detector. The order

of the column 1 are the compass operator with NMS, the compass operator with NMS and Medina *et al.* method, MVD detector, MVD detector with thinning process and Medina *et al.* method, Color Canny detector, RCMG detector with thinning process and Medina *et al.* method, and our automatic color edge detector. The column 2 to column 5 represents the quantitative evaluations of FOM, TPR, TNR, and NACC in percentage, respectively. For the criteria, a detector, which can detect less erroneous, thin, and continuous edges, will get high values of the FOM and NACC.

TABLE 4.4
The average evaluation results of the eleven 128×128 synthetic color images detected by the following detectors

Method	FOM (%)	TPR (%)	TNR (%)	NACC (%)
Compass with NMS with manual thresholding	99.48_4	96.87	99.87	98.37_4
Compass with NMS and Medina *et al.* method	98.84_5	96.80	99.93	98.37_4
MVD with manual thresholding	93.86_6	63.18	100.00	81.59_7
MVD with thinning and Medina *et al.* method	99.68_1	98.10	99.91	99.01_2
Color Canny with manual thresholding	83.79_7	70.65	97.47	84.06_6
RCMG with thinning and Medina *et al.* method	99.49_3	98.11	99.87	98.99_3
Our method	99.54_2	99.98	99.96	99.97_1

TABLE 4.5

The average evaluation results of the eleven 256×256 synthetic color images detected by the following detectors

Detector	FOM (%)	TPR (%)	TNR (%)	NACC (%)
Compass with NMS with manual thresholding	98.99_5	93.98	99.92	96.95_5
Compass with NMS and Medina *et al.* method	99.06_4	94.50	99.96	97.23_4
MVD with manual thresholding	93.86_6	63.20	99.99	81.60_7
MVD with thinning and Medina *et al.* method	99.70_1	98.53	99.91	99.21_3
Color Canny with manual thresholding	89.70_7	71.59	98.46	85.03_6
RCMG with thinning and Medina *et al.* method	99.62_2	98.53	99.91	99.22_2
Our method	99.40_3	99.96	99.96	99.96_1

TABLE 4.6

The average evaluation results of the total synthetic color images detected by the following detectors

Detector	FOM (%)	TPR (%)	TNR (%)	NACC (%)
Compass with NMS with manual thresholding	99.23_4	95.43	99.89	97.66_5
Compass with NMS and Medina *et al.* method	98.95_5	95.65	99.95	97.80_4
MVD with manual thresholding	93.86_6	63.19	99.99	81.59_7
MVD with thinning and Medina *et al.* method	99.69_1	98.31	99.91	99.11_2
Color Canny with manual thresholding	86.74_7	71.12	97.97	84.54_6
RCMG with thinning and Medina *et al.* method	99.56_2	98.32	99.89	99.11_2
Our method	99.47_3	99.97	99.96	99.97_1

A noisy edge map may be high performance in the FOM evaluation due to the FOM only considers the accuracy of edge points and uses a scaling constant α for the penalty between smeared and offset edges. In other hand, the NACC calculates not only the accuracy of edge points but also the accuracy of non-edge points and rigorously forbids the deviation between ideal and detected edge (non-edge) points. Thus, although both MVD and RCMG with thinning and Medina *et al.* method are better than our method for the FOM evaluation, TPR and TNR shows the fact that they produce more smeared edge points and misses more ideal edge points than our method. Indeed, the NACC evaluation supply more reliable results by using the TPR and TNR, and our method is the best one in the NACC evaluation.

4.3.2 Comparison in Nature Color Images

In this section, we will compare our method in nature color images with other detectors mentioned above. Unlike the synthetic images, we can not use the FOM evaluation or ROC analysis to provide the absolute quality measures when GT images in real world images are both difficultly and subjectively chosen, but we can provide the information for relatively robustness and reliability.

Figs. 4.16 and 4.17 show the edge detection results of the Peppers and Lena image. We also use the parameter $\sigma = 0.94$ for the compass operator, $k = 2$ and $l = 4$ for MVD detector. For Fig. 4.16(b), the hysteresis threshold, $t_{low} = 0.275$ and $t_{high} = 0.55$, are chosen subjectively for the compass operator with NMS, and the very noisy edge result for thresholding by Medina *et al.* method is shown as Fig. 4.16(c). Both MVD result, where thresholding by hysteresis threshold $t_{low} = 15$ and $t_{high} = 30$ shown as Fig. 4.16(d) and thresholding by Medina *et al.* method with

(a)

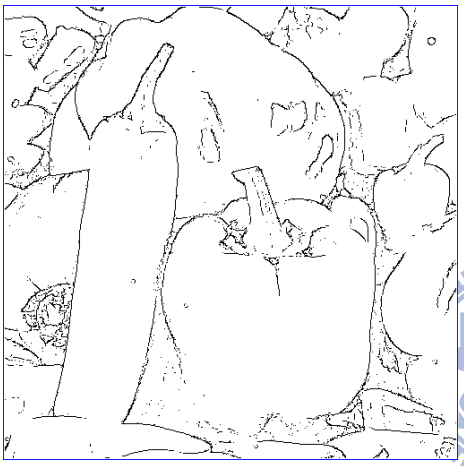

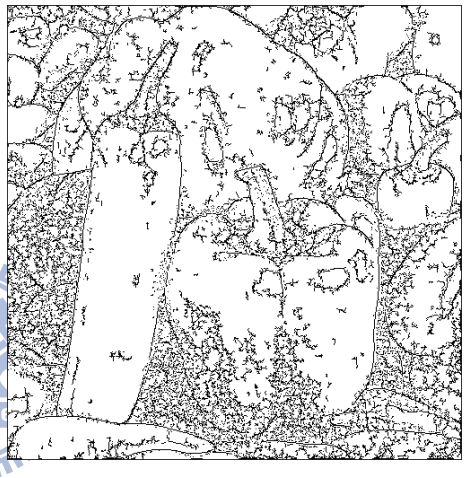

(b) (c)

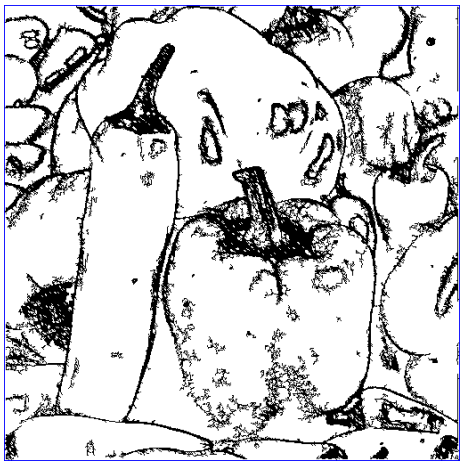

(d) (e)

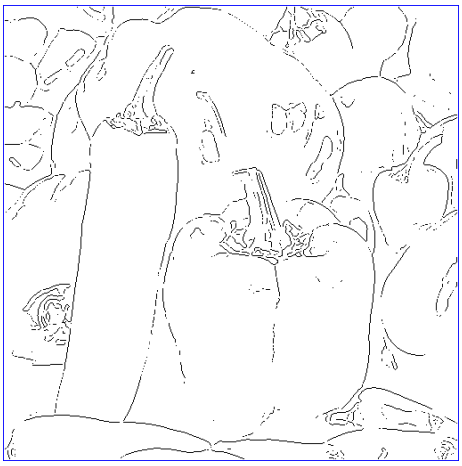

(f)

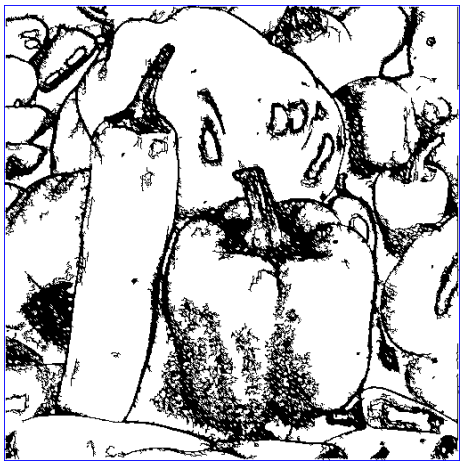

(g)

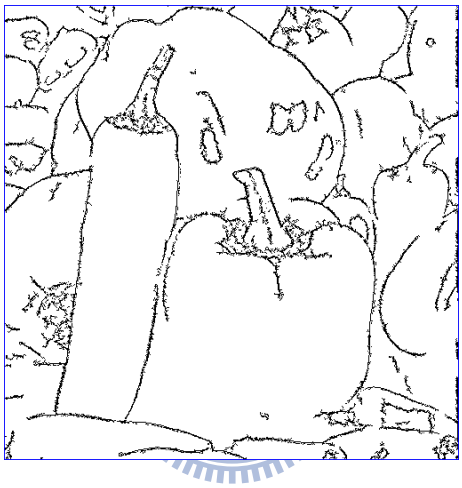

(h)

Fig. 4.16. Edge detection results of the Peppers image detected by different color edge detectors. (a) Original image. (b) Compass result, (c) The compass operator with NMS and thresholding by Medina *et al.* method. (d) MVD result. (e) MVD with thinning process and thresholding by Medina *et al.* method. (f) Color Canny result. (g) RCMG with thinning process and thresholding by Medina *et al.* method. (h) Our automatic color edge detector.

thinning process shown as Fig 4.16(e), detect more true edges but less noise although they provide the very thick responses. Figs. 4.16(f)－(h) show the result of Color Canny, RCMG and our method. Color Canny and our method not only provide

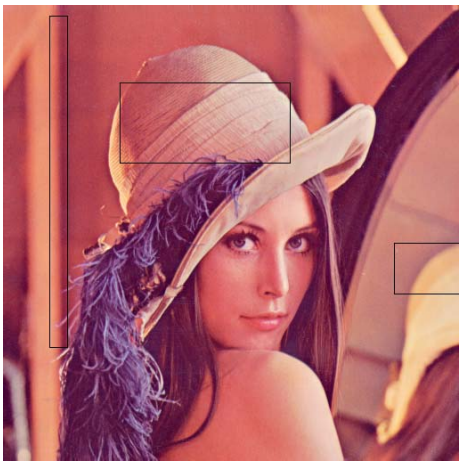

(a)

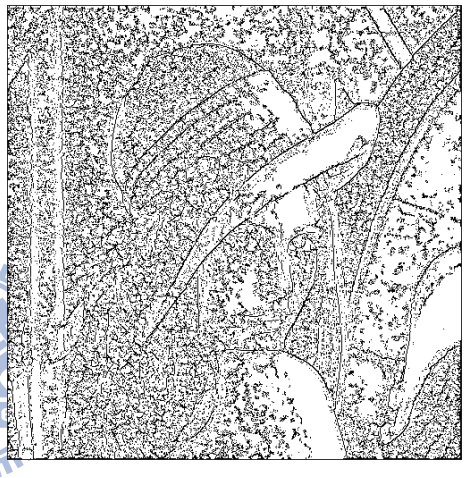

(b) (c)

(d) (e)

(f)

(g)

(h)

Fig. 4.17. Edge detection results of the Lena image detected by different color edge detectors. (a) Original image. (b) Compass result, (c) The compass operator with NMS and thresholding by Medina *et al.* method. (d) MVD result. (e) MVD with thinning process and thresholding by Medina *et al.* method. (f) Color Canny result. (g) RCMG with thinning process and thresholding by Medina *et al.* method. (h) Our automatic color edge detector.

Thinner and less noisy edges but also catch the boundaries such as the three marked black ellipse regions that are difficult to distinguish.

Another experiment for compared results is shown as Fig. 4.17. We are

interesting in comparing the marked rectangle regions. Figs. 4.17(c) and (e) detect more edge in these regions, but they also provide too much noise. In the left rectangle region, the compass operator shown as Fig. 4.17(b) produces stronger response for edge detection, but in the regions of the middle and right rectangles, the results of Figs. 4.17(f) and (h) detected by color Canny and our method are better than the compass operator.

Chapter 5 Conclusion

In this thesis, we have proposed to apply vector order statistics and fuzzy gradient to our automatic color edge detection. By using the fuzzy derivative estimation, the fuzzy rules are fired to consider the gradient direction of every processing pixel. Additionally, the shape of the membership function is adapted to the local variation around the processing pixel. Therefore, the proposed detector improve the drawbacks of the original VMD detector due to the gradient directions are exactly estimated, and our thresholding method choose an reasonable parameter set from all possible values and find the best hysteresis threshold set within it.

Experimental results have shown that our automatic color edge detection techniques produce excellent edge detection accuracy in the synthetic and nature images. In this way, the performances of higher level image processing tasks such as segmentation and object recognition can be improved because of the improvement of edge detection result.

References

[1] J. Canny, “A computational approach to edge detection,” *IEEE Trans. Pattern Anal. Mach. Intell.*, vol. 8, no. 6, pp. 679–698, 1986.

[2] C. L. Novak and S. A. Shafer, “Color edge detection,” in *Proc. of DARPA Image Understanding Workshop*, 1987, pp. 35–37.

[3] P.E. Trahanias and A.N. Venetsanopoulos, “Color edge detection using vectororder statistics,” *IEEE Trans. Image Process*., vol. 2, no. 2, pp. 259–264, April 1993.

[4] P.E. Trahanias and A.N. Venetsanopoulos, “Vector order statistics operators as color edge detectors,” *IEEE Trans. Syst., Man, Cybern., B*, vol. 26, no. 1, pp. 135–142, February 1996.

[5] D. Van De Ville, M. Nachtegael, D. Van der Weken, E.E. Kerre, W. Philips, and I. Lemahieu, “Noise reduction by fuzzy image filtering,” *IEEE Trans. Fuzzy Systems*, vol. 11, no. 4, pp.429–436, August 2003.

[6] S. Schulte, V. De Witte, M. Nachtegael, D. Van der Weken, E.E. Kerre, “Fuzzy random impulse noise reduction method,” *Fuzzy Sets and Systems*, vol.158, pp.270–283, February 2007.

[7] M. A. Ruzon and C. Tomasi, “Edge, junction, and corner detection using color distributions,” *IEEE Trans. Pattern Anal. Mach. Intell.*, vol. 23, no.11, pp. 1281–1295, Nov. 2001.

[8] J. Scharcanski and A.N. Venetsanopoulos, “Edge detection of color images using directional operators,” *IEEE Trans. Circuits Syst. Video Technol*., vol. 26, no. 1, pp. 135–142, February 1996.

[9] A. N. Evans and X. U. Liu, “A morphological gradient approach to color edge detection,” *IEEE Trans. Image Process.*, vol. 15, pp. 1454–1463, 2006.

[10] A. Cumani, “Efficient contour extraction in color images,” in *ACCV ’98: Proceedings of the Third Asian Conference on Computer Vision*, London, UK, 1998, vol. 1, pp. 582–589, Springer-Verlag.

[11] N. Otsu, “A threshold selection method from grey-level histograms,” *IEEE Trans. Syst. Man Cybern.*, vol. SMC-9, pp. 62–66, 1979.

[12] P. L. Rosin, “Unimodal thresholding,” *Pattern Recognit.*, vol. 34, pp.2083–2096, 2001.

[13] R. Rakesh, P. Chaudhuri, and C. A. Murthy, “Tresholding in edge detection: A statistical approach,” *IEEE Trans. Image Process.*, vol. 13, pp. 927–936, 2004.

[14] H. A. David, *Order Statistics*. New York: Wiley, 1980.

[15] V. Barnett, “The ordering of multivariate data,” *J. Royal Statistical Society A*, vol. 139, Part 3, pp. 318–343, 1976.

[16] J. Astola, P. Haavisto and Y. Neuvo, “Vector median filters,” *Proc. IEEE*, vol. 78, pp. 678–689, April 1987.

[17] Y. Yitzhaky and E. Peli, “A method for objective edge detection evaluation and detector parameter selection,” *IEEE Trans. Pattern Anal. Mach. Intell.*, vol. 25, pp. 1027–1033, 2003.

[18] R. Medina-Carnicer, A. Carmona-Poyato, R. Muñoz-Salinas, and F. J. Madrid-Cuevas, “Determining hysteresis thresholds for edge detection by combining the advantages and disadvantages of thresholding methods,” *IEEE Trans. Image Process.*, vol. 19, no. 1, pp.165–173, January 2010.

[19] T. Fawcett, “An introduction to ROC analysis,” *Pattern Recognition Letters*, vol. 27, no. 8, pp. 861–874, 2006.

[20] I. Abdou. And W. Pratt, “Quantitative design and evaluation of enhancement/thresholding edge detectors,” *Proc. IEEE*, vol. 67, pp. 753–763, 1979.

[21] M. Heath, S. Sarkar, T. Sanocki, and K.W. Bowyer, “Comparison of Edge Detectors: A Methodology and Initial Study,” Computer Vision and Image Understanding, vol. 69, no. 1, pp. 38-54 Jan. 1998.

[22] K. Bowyer, C. Kranenburg, and S. Dougherty, “Edge Detector Evaluation Using Empirical ROC Curves,” Computer Vision and Image Understanding, vol. 84, no. 1, pp. 77-103, Oct. 2001.

[23] N. L. Fernández-García, A. Carmona-Poyato, R. Medina-Carnicer, and F. J. Madrid-Cuevas, “Automatic generation of consensus ground truth for the comparison of edge detection techniques,” *Image Vis. Comput.*, vol. 26, pp. 496–511, 2008.